SERS- and electrochemically active 3D Plasmonic liquid marbles for molecular-level spectroelectrochemical investigation of microliter reactions

Koh, Charlynn Sher Lin; Lee, Hiang Kwee; Phan-Quang, Gia Chuong; Han, Xuemei; Lee, Mian Rong; Yang, Zhe; Ling, Xing Yi

2017

Koh, C. S. L., Lee, H. K., Phan-Quang, G. C., Han, X., Lee, M. R., Yang, Z., & Ling, X. Y. (2017). SERS- and electrochemically active 3D Plasmonic liquid marbles for molecular-level spectroelectrochemical investigation of microliter reactions. Angewandte Chemie International Edition, 56(30), 8813-8817. doi:10.1002/anie.201704433

https://hdl.handle.net/10356/143425

https://doi.org/10.1002/anie.201704433

COMMUNICATION

SERS- and Electrochemically-Active 3D Plasmonic Liquid Marble for Molecular-Level Spectroelectrochemical Investigation of Microliter Reaction**

Charlynn Sher Lin Koh,[a] Hiang Kwee Lee,[a],[b] Gia Chuong Phan-Quang,[a] Xuemei Han,[a] Mian Rong Lee,[a] Zhe Yang,[a] Xing Yi Ling*[a]

Abstract: Liquid marbles are emerging microreactors due to their isolated environment and flexibility of materials used. Herein, we demonstrate plasmonic liquid marble (PLM) as the smallest spectroelectrochemical microliter-scale reactor for concurrent spectro- and electrochemical analyses. We exploit PLM's three-dimensional Ag shell as bifunctional surface-enhanced Raman scattering (SERS) platform and working electrode for redox process modulation. The combination of SERS and electrochemistry (EC) capability enable in situ molecular read-out of transient electrochemical species, and elucidation of potential-dependent and multi-step reaction dynamics. The 3D configuration of our PLM-based EC-SERS system exhibits 2-fold and 10-fold superior electrochemical and SERS performance than conventional 2D platforms. The rich molecular-level electrochemical insights and excellent EC-SERS capabilities offered by our 3D spectroelectrochemical system is pertinent in charge transfer processes.

Liquid marbles are emerging lab-on-a-droplet platforms which efficiently isolate liquid reaction medium within a three-dimensional (3D) particle shell to impart robustness and overcome rapid evaporation typical in small-volume processes.[1] These versatile microreactors can be further imbued with function-specific attributes, such as photothermal and catalytic properties,[2] via the selection of active encapsulating solids, and have diverse (bio)chemical applications.[3] For instance, the plasmonic liquid marble (PLM) constructed using metallic nanoparticles has enabled the elucidation of critical reaction mechanism and dynamics using surface-enhanced Raman spectroscopy (SERS).[3b]

Despite the vast potentials offered by liquid marbles, these reactors are limited to spontaneous chemical reactions driven intrinsically by the presence of multiple reactive reagents. Electrochemical (EC) reactions form the basis of important energy- and environmental-related applications, such as energy storage mechanisms in chemical batteries,[4] and charge transfers in biochemical processes.[5] The fusion of liquid marble with electrochemistry is hence tantalizing to expand its application for electrochemical activation of small-volume inert reactions. The spherical shell of the liquid marble also provides a unique geometry as a working electrode. However, it remains challenging to perform EC in liquid marbles due to the dearth of in-depth understanding of charge transfer properties across liquid marbles and the technical difficulties in incorporating commercial three-electrode system in a microliter droplet. Notably, due to its inability in giving structural and adsorption data, EC are often coupled with molecular-specific spectroscopy, like SERS, to provide unequivocal identification of species for comprehensive understanding of complicated redox systems.[6] A typical method to fabricate SERS-active electrodes is via metal oxidation-reduction cycle[7] often leads to inconsistent surface roughness and suffers from reproducibility issues. While methods are developed to prepare electrodes with tunable metallic nanostructured surfaces, e.g. metal film over nanosphere[8] and sphere segment void nanostructured films,[9] these designs often require multiple-step protocols and is difficult for the electrodes to be miniaturized down to microliter scale.

Herein, we demonstrate the PLM as an ideal micro test-bed for spectroelectrochemical analysis capable of circumventing the aforementioned limitations, leveraging on the plasmonic and electrically conductive metallic shell as a bifunctional SERS- and EC-active platform. Exploiting the Ag shell as the first miniaturized 3D spherical working electrode, we first highlight the ability of the PLM soft metallic shell to perform EC reactions at precise voltages calibrated using standard redox probe, and demonstrate the excellent reproducibility of our improvised three-electrode microsystem over extended analysis period. PLM is then showcased as the smallest spectroelectrochemical cell capable of offering potential-dependent read-out of molecular vibrational fingerprints and electro-thermodynamics simultaneously, using the colorless rutheniumhexammmine (III) chloride ($Ru(NH_3)_6Cl_3$) and environmental toxin methylene blue (MB^+) as model compounds. Remarkably, the synergistic electrochemical and SERS capability of the PLM enables the elucidation of critical insights on EC reaction mechanism, molecular structural changes, and quantitative temporal concentration for kinetic dynamics that cannot be accomplished with EC or SERS alone. Finally, we exemplify the importance of our unique 3D electrode by comparing the superior EC and SERS performance of PLM over conventional 2D micro-platforms.

HCl-treated Ag nanocubes (edge length of 133 ± 9 nm; Figure 1A, S1) are used as the metallic building blocks of the PLM due to the superior SERS enhancement arising from the intense localized electromagnetic fields at the sharp edges,[10] and also 1.2-fold higher electrical conductivity compared to as-synthesized, polyvinylpyrrolidone-capped Ag nanocubes (Figure S2, S3). Upon the addition of a 40 µL aqueous droplet, the Ag nanocubes

[a] C.S.L. Koh, H.K. Lee, G.C. Phan-Quang, Dr X. Han, M.R. Lee, Z. Yang, Prof X.Y. Ling
Division of Chemistry and Biological Chemistry, School of Physical and Mathematical Sciences, Nanyang Technological University, Singapore 637371 (Singapore)
E-mail: xyling@ntu.edu.sg

[b] H.K. Lee
Institute of Materials Research and Engineering, Agency for Science, Technology and Research (A*STAR), 2 Fusionopolis Way, Innovis, No. 08-03, Singapore 138634

[**] X.Y.L. thanks the financial support from National Research Foundation, Singapore (NRF-NRFF2012-04), Nanyang Technological University's start-up grant, and Singapore Ministry of Education, Tier 1 (2016-T1-001-101) and Tier 2 (MOE2016-T2-1-043) grants. C.S.L.K., G.C.P- Q and M.R.L. acknowledges support from Nanyang Presidential Graduate Scholarship. H.K.L. thanks the graduate scholarship from A*STAR, Singapore.

Supporting information for this article is given via a link at the end of the document

suspended in decane spontaneously assemble on the microdroplet surface to form a 3D encapsulating shell (Figure 1A) driven by the large interfacial energy between the aqueous and organic decane phases.[11] The Ag nanocube shell exhibits the appearance of bulk silver arising from the uniform and compact array at optimized Ag-to-water ratio of 7.5 µg/µL (shell thickness ~ 500 nm; Figure S4). X-y hyperspectral SERS evaluation of PLM demonstrate its intense SERS activity with an analytical enhancement factor (AEF) of 2.6 × 10^8, and excellent homogeneity (< 10 % relative standard deviation (%RSD)) across a large evaluation area (165 µm × 65 µm, > 1300 spectra; Figure 5, S6). The intense and homogeneous SERS responses directly affirm the compactness of the plasmonic shell, where plasmonic coupling of adjacent Ag nanoparticles in x-, y- and z- spatial direction create dense and strong electromagnetic hot-spots evenly distributed around PLM. Hereon, all experiments are conducted in a 40 µL droplet using the optimal Ag-to-water ratio of 7.5 µg/µL to ensure electrical continuity and high SERS readout.

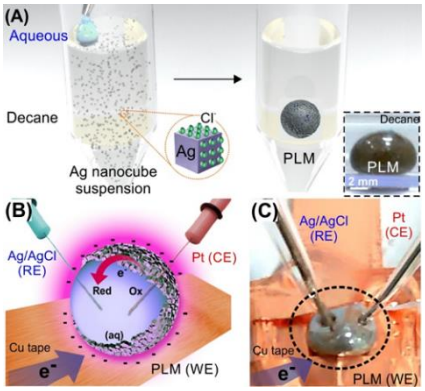

Figure 1. (A) Fabrication of PLM. Inset shows digital image of PLM. (B) Schematic on the use of Ag shell as 3D working electrode (WE). (C) Digital image of the EC-SERS set up.

We then evaluate the PLM as a conductive 3D working electrode (WE) by performing CV using electroactive $Ru(NH_3)_6Cl_3$ as our model probe dissolved in the enclosed aqueous microdroplet (Figure 1B, Figure 2). A three-electrode system is improvised to allow precise regulation of applied voltage. Pt electrode and Ag/AgCl wire serve as a counter and quasi-reference electrode, respectively (Figure 1C, S7, S8). In a forward scan, we observe the emergence of a cathodic peak at –0.28 V as the applied potential is regulated systematically from –0.05 to –0.5 V (Figure 2B). An anodic peak subsequently evolved at –0.19 V as the applied potential is reversed from –0.5 V back to the initial –0.05 V. The peak separation is determined at 0.09 V, which is comparable with literature using similar droplet cell setup.[12] These finding clearly reflects a one-electron redox process involving the electroreduction of $Ru(NH_3)_6Cl_3$ to $Ru(NH_3)_6Cl_2$. Furthermore, we note the similar peak currents of cathodic and anodic electrochemical responses quantified at 27 and 30 µA, respectively, which can be attributed to the excellent reversibility of $Ru(NH_3)_6Cl_3$ electroreduction. Such stable and well-defined redox peaks of our redox probe when using PLM as electro-active microreactor indicates the efficient electron transfer between the electrode and electroactive species. PLM functioning as a working electrode is again affirmed on comparison with a control insulating silica liquid marble, which reveals featureless

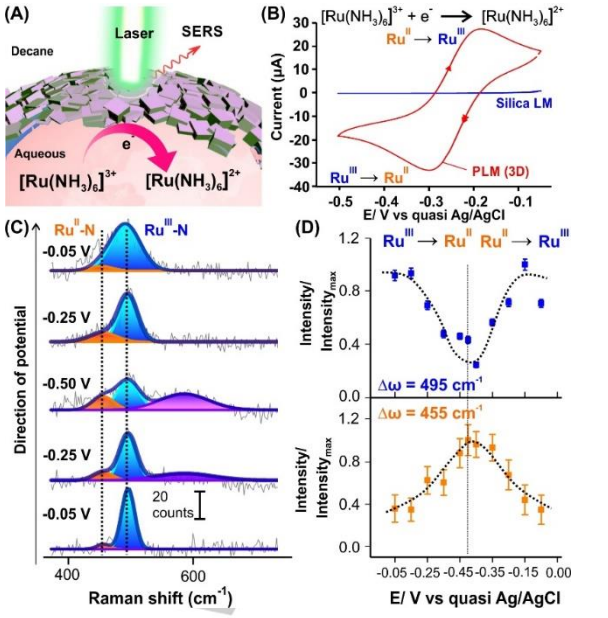

Figure 2. (A) Scheme depicting EC-SERS investigation using PLM, (B) CV of 3D PLM shell (red) and 2D Ag nanocube-based WE (black), and silica liquid marble (SLM; blue). (C) SERS spectra changes when applied potential is scanned from -0.05 to -0.5 V and back. (D) Plot of SERS intensity as a function of potential at the 495 cm^{-1} band (blue) and 455 cm^{-1} band (orange). The bands are assigned to the Ru^{III}-N and Ru^{II}-N stretchings, respectively.

and negligible EC responses, signifying no redox reaction occurring under identical CV conditions. The 3D metallic shell also demonstrates ~ 2-fold higher peak current (~ 27 µA) relative to the planar WE (~ 18 µA) formed by dropcasting Ag nanocubes onto copper tape, which directly denotes the superior electrochemical performance of 3D PLM electrodes over conventional planar counterpart. This is due to the efficient utilization of electrode materials with higher specific electrode surface area in a 3D configuration (Supporting Text S1). Furthermore, the PLM's shell is highly durable, as evident from both the excellent consistency of the measured current over 100 cycles of CV (%RSD ≤ 3%) and preservation of Ag nanocubes' morphology (Figure S9). The similar symmetric shape of the CV compared to bulk EC also indicates minimal distortions arising from the high current density of the small CE (Figure S10). Our results therefore collectively emphasize the immense potential of PLM as a robust and efficient microsystem for practical EC applications.

PLM as a microliter-scale spectroelectrochemical cell is further demonstrated by in situ reaction monitoring using SERS which further provides both molecular-level identification and quantification of the entire electron-transfer processes occurring at the electrode surface. At the initial potential of –0.05 V, we observe one SERS band centred at 495 cm^{-1} with a maximum intensity of 44 counts (Figure 2C, D). The SERS intensity of the 495 cm^{-1} band remains relatively constant even as potential decreases to –0.15 V. As the potential reaches –0.25 V, the SERS intensity of 495 cm^{-1} band begins to decrease with the concomitant emergence of a new vibrational feature at a more red-shifted region of 455 cm^{-1}.[7b, 8a] Further regulation of applied potential to –0.5 V leads to the 4-fold decrease of 495 cm^{-1} SERS intensity, whereas the band at 455 cm^{-1} increase by 3-folds

(Figure 2C, D). The SERS spectral changes are indicative of a single-step reaction occurring at the electrode surface. The band at 495 cm^{-1} can be assigned to the Ru^{III}- N stretching while the 455 cm^{-1} band arises due to the Ru^{II}-N stretching [7b, 8a]. This agrees with the fact that as the charge on Ru decreases, the polar interaction between amine ligand and Ru^{II} metal center is reduced. Consequently, Ru-N bond strength decreases (lower vibrational force constant) and causes the bond to vibrate at lower frequency compared to Ru^{III}. The lower intensity of Ru^{II}-N stretching could be due to the decrease in polarizability of the bond arising from the reduction of Ru^{3+} to Ru^{2+}. Our SERS observations therefore clearly correlate to the CV cathodic peak at –0.28 V where $Ru(NH_3)_6^{3+}$ is reduced to $Ru(NH_3)_6^{2+}$. This is further supported by the appearance of a broad NH_3 rocking mode (585 cm^{-1}) at -0.25 V,[13] which gradually experiences an increase in its intensity at more negative potential. Such phenomenon is due to electric field-induced adsorption reorientations of the complex, whereby the closer proximity of ammine ligands to the Ag surface enhances its SERS responses. It is also noteworthy that changes in these spectral features are reverted as the applied potential is tuned from –0.5 to the initial –0.05 V, a clear indication on the reversibility of the redox reaction. SERS intensity of Ru^{III}-N mode at 495 cm^{-1} increases back to its maximal intensity while the Ru^{II}-N vibrational mode diminishes to negligible intensity (<3 counts). Collectively, SERS- and electrically-active PLM is important to track both molecular events and concentration changes during electrochemical reaction at the electrode surface, notably using just 40 µL of the reaction solution.

Heterogeneous electroreduction of methylene blue (MB^+) toxin is also performed as a second electrochemical model to demonstrate the versatility of our system in analysing multi-electron redox systems (Figure 3, S11). As the potential is cycled between –0.1 and –1 V, MB^+ exhibits two cathodic peaks at –0.42 and -0.56 V (peak 1 and 2) and two anodic peaks at –0.47 and –0.31 V (peak 3 and 4) during the forward (–0.1 to –1 V) and reverse scans, respectively (Figure 3B). Peaks 1 – 4 possess complementary peak currents of 8.7, 14.0, 6.5, and 13.0 µA, respectively. These peaks and their matching currents jointly reflect the two one-electron transfers from the applied current to MB^+, resulting in the final reduced product, leucomethylene blue (LMB) (Figure 3A). MB^+ first receives an electron to form radical $MB^•$ (peak 1; MB^+ → $MB^•$). This is followed by protonation of $MB^•$ to yield radical cation ($HMB^{•+}$), which is subsequently reduced by receiving another electron to produce LMB (peak 2; $HMB^{•+}$ → LMB). Correspondingly, the reversed reactions of LMB oxidation to $HMB^{•+}$, and to the initial MB^+ are assigned to peak 3 (LMB → $HMB^{•+}$) and peak 4 ($MB^•$ → MB^+), respectively.[14]

We highlight the importance of PLM's Ag shell as an active electron relay center to resolve multi-step electron transfers by comparing the electrochemical responses with control experiment involving naked reaction microdroplet placed on top of the Cu tape (Figure 3B). The control CV reveals only one anodic peak and overall sluggish electron transfer, reflecting an irreversible process during the oxidation of LMB back to MB in the absence of Ag shell. This evidently emphasizes the importance of Ag nanocube shell as an efficient electron transfer modulator between the externally-applied current to electro-active species which enables a more efficient reduction and its subsequent reversible oxidation process, resulting in enhanced degradation and representative EC investigations.[15]

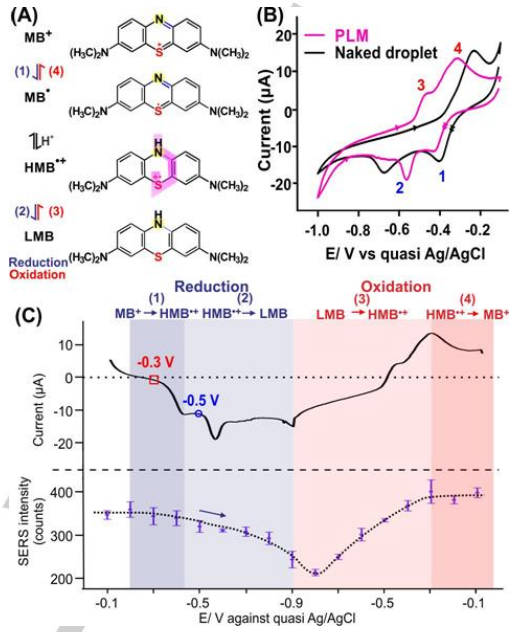

Figure 3. (A) Heterogeneous reduction mechanism of MB. Colored regions highlight the chemical moiety that undergo molecular changes during the redox reaction. (B) CV of aqueous MB when isolated within PLM (red), and without PLM (blue). (C) Correlation of the electrochemical responses from CV (top) with SERS intensity (bottom) of 1639 cm^{-1} band.

Next, we quantitatively track the structural changes of MB^+ at the Ag nanocube shell using in situ SERS, and relate the molecular-level information with the EC insights from the CV (Figure 3C, S12). The SERS measurement is performed at 0.1 V intervals when cycled between –0.1 to –0.9 V. In the reduction pathway, the nitrogen atom (yellow) of $MB^•$ gains a proton (H^+) and results in a structural change of the molecule where the C=N bond is reduced to C–N–H in LMB (Figure 3A). Hence, the sharp and intense C=N stretching mode at 1639 cm^{-1} is selected to represent the presence of MB^+ (and also $MB^•$) during the potential-dependent SERS investigation.[16] In the forward scan from –0.1 to –0.5 V, the SERS intensities remain constant (~ 347 counts, < 3 % change) because C=N bond remains present even as MB^+ is reduced to $MB^•$ at –0.42 V. This is followed by the onset reduction of SERS intensity to a minimum of 213 counts at –0.8 V after applied potential is reversed at –0.9 V. On reversal of the applied potential, the SERS intensity increases and eventually reaching a plateau of ~ 393 counts after –0.3 V, corresponding to the reduction peak of $MB^•$ to MB^+ in the CV. Such observations can be explained using the Nernst equation, where the ratio reactant:product is dependent on the applied potential (Figure S12). Hence, upon reversal of potential to less negative potentials, the reduction of MB to LMB still occurs but the ratio of [LMB]/[MB] decreases. Thus is also in close agreement with previous spectroelectrochemical investigations.[9c, 17] Owing to the surface-sensitive nature of SERS, these intensities are directly proportional to MB^+ concentration at the Ag shell,[18] and the spectral changes reflect the potential-dependent molecular changes during the MB^+ redox, congruent to the EC insights derived from CV. Quantitative examination using SERS thus

holds an advantage over UV-vis absorption spectroscopy, where the latter usually reveals bulk concentration changes that are not representative of the actual concentration profile at the electrode interface, especially for diffusion-limited analysis.[19] More importantly, structural changes, which cannot be obtained from UV-vis spectroscopy, can also be identified from the changes of molecular fingerprints during the electroreduction of MB^+ to LMB. For example, the C=N–C ring stretching (1410 cm^{-1}) that is only present in MB^+ attenuates by 3-folds while the weak C–N–C stretching mode (1524 cm^{-1}) belonging to LMB red-shift by 6 cm^{-1} and increases by 2-folds due to the formation of LMB (Figure S13). We exclude any potential EC and SERS interference from the Ag shell, electrolyte or systematic signal fluctuations from the consistent and featureless spectra in the control (Figure S14). The onsite read-out of potential-induced molecular transformation clearly demonstrates the immense advantages of PLM to definitively identify EC species in its native reaction environment.

In addition, PLM also offers ultrasensitive SERS activities for the determination of potential-dependent reaction kinetics. Such evaluation is challenging in typical standalone electrochemical systems due to their limited sensitivity for rapid quantification of time-dependent species' concentration.[20] Using the time dependent intensity change at –0.5 V, we note the exponential decrease of SERS intensity, reaching an eventual plateau at 310 counts after 9 min (Figure S15). Such exponential relationship can be modelled using a pseudo-first order kinetics equation of $I = 307 + 38.6e^{-0.240t}$, where I is the intensity in counts and t is the time in minutes, and rate constant is 0.240 min^{-1}. Collectively, our results demonstrate the importance of the synergism of molecular-specific vibrational spectroscopy with EC to provide critical molecular-level and quantitative insights.

Lastly, we demonstrate superior SERS and EC capability of the PLM over controls involving conventional 2D micro-platform and non-plasmonic active silica liquid marble (SLM; Figure 4A-C). Notably, the SERS intensity using PLM is >10-fold higher than its 2D counterpart (Figure 4D, E), prepared by the pre-deposition of Ag nanocubes onto the copper tape, while SLM exhibits negligible SERS response. These two control micro-platforms therefore emphasize the importance of 3D Ag nanocube shell in PLM for SERS enhancements. The better SERS performance in PLM over other systems stems from the direct sensing of the analyte at the top of PLM's Ag nanocube shell, which enables a more accessible pathway for the excitation laser to reach the SERS platform and effective collection of Raman scattered lights back to the detector. In the contrary, the laser and Raman scattered light are required to travel through the aqueous solution to reach the control 2D SERS platform at the bottom and detector, respectively, which could be both attenuated by the light-absorbing dye solution and impede the successful recording of vital molecular signatures. The remarkable SERS capability of PLM is again highlighted via its ~ 5-fold higher sensitivity (115 counts/ 0.1 V) compared to the conventional 2D control (24 counts/ 0.1 V) (Figure 4F), hence allowing the accurate distinction of minute concentration changes. The efficient laser excitation and collection of Raman scattered light facilitated by the 3D configuration is therefore crucial in the ultrasensitive analysis of voltage-induced structural changes. This is especially critical in temporal SERS measurements, where any low intensity and its associated high error (average %RSD = 63 %) of the SERS measurements could severely hinder the representative elucidation of temporal information and reaction kinetics (Figure 4G). Collectively, these comparisons therefore clearly reflect the ultrasensitivity of the PLM-based spectroelectrochemical micro-reactor necessary for efficient EC-SERS characterization, especially for EC processes with low species concentrations and/or weak Raman scattering.

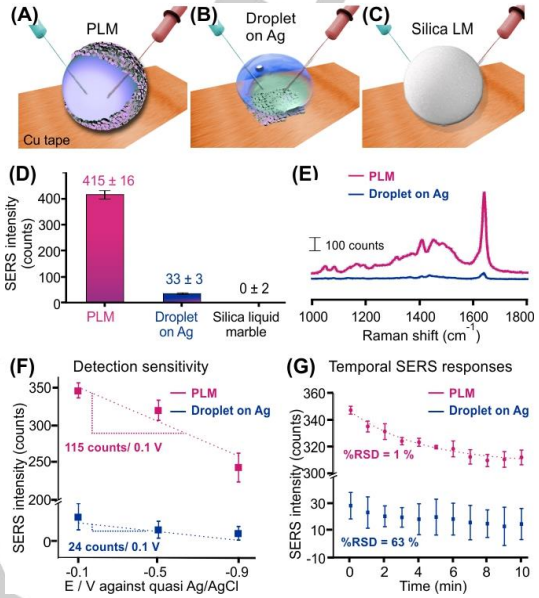

Figure 4. Scheme of different WE using (A) PLM, (B) 2D layer Ag nanocubes deposited on Cu tape, and (C) SLM. (D) SERS intensity of MB using (A-C). (E-G) Comparing the performance of PLM (pink) and 2D Ag nanocube layer (blue) as a spectroelectrochemical platform; (E) SERS spectra of MB at non-reducing and reducing potentials. (F) Plot of SERS intensity changes with voltage. (G) Temporal SERS intensities of aqueous MB solution at –0.5 V. All intensities are obtained based on MB's 1639 cm^{-1} C=N mode.

In conclusion, we utilize the highly versatile PLM as an isolated and smallest 3D miniature reactor for simultaneous molecular-level analysis of EC processes. Together with its dual functionalities as SERS-active platform and working electrode, PLM's Ag shell also faciliates electron relay and demonstrates immense potential for real-time molecular-level identification of transient species, using the electrodegradation of a toxin as a model. These insights is crucial for elucidation of tandem EC reactions dynamics, which is not possible via standalone EC methods. More importantly, our novel 3D electrode exhibits 2-fold and 10-fold better electrochemical- and SERS-activities than their conventional 2D counterparts. Despite the potential window limit of Ag, the rich information and excellent performance offered by PLM still serves as an important proof of concept, which can be easily extended to vast nanomaterials of various materials or shape to better cater for specific experiment conditions. This finding is valuable to impact future design of 3D electrode system for enhanced electrochemical performance relevant in the broad applications in environmental conservation, energy harvesting, and biochemical charge transfer.

Keywords: spectroelectrochemistry • Ag nanoparticles • liquid marble • in-situ SERS • 3D electrode

[1] aP. Aussillous, D. Quere, *Nature* **2001**, *411*, 924-927; bE. Bormashenko, *Langmuir : the ACS journal of surfaces and colloids* **2017**, *33*, 663-669.

[2] aW. Gao, H. K. Lee, J. Hobley, T. X. Liu, I. Y. Phang, X. Y. Ling, *Angew Chem Int Edit* **2015**, *54*, 3993-3996; bS. Yang, X. Zhu, S. Zhou, S. Wang, Z. Feng, Y. Wei, H. Miao, L. Guo, F. Wang, G. Zhang, X. Gu, X. Mu, *Dalton Trans* **2014**, *43*, 2521-2533.

[3] aT. Arbatan, L. Li, J. Tian, W. Shen, *Adv Healthc Mater* **2012**, *1*, 80-83; bX. Han, H. K. Lee, Y. H. Lee, W. Hao, Y. Liu, I. Y. Phang, S. Li, X. Y. Ling, *J. Phys. Chem. Lett.* **2016**, 1501-1506; cJ. Tian, T. Arbatan, X. Li, W. Shen, *Chem. Commun.* **2010**, *46*, 4734-4736.

[4] Z. Yang, J. Zhang, M. C. W. Kintner-Meyer, X. Lu, D. Choi, J. P. Lemmon, J. Liu, *Chem. Rev.* **2011**, *111*, 3577-3613.

[5] A. Efrati, C.-H. Lu, D. Michaeli, R. Nechushtai, S. Alsaoub, W. Schuhmann, I. Willner, *Nat. Energy* **2016**, *1*, 15021.

[6] aC. P. Byers, B. S. Hoener, W.-S. Chang, S. Link, C. F. Landes, *Nano Lett.* **2016**, *16*, 2314-2321; bS. Yasuda, S. Hoshina, S. Chiashi, S. Maruyama, K. Murakoshi, *Nanoscale* **2016**, *8*, 19093-19098.

[7] aJ. F. Owen, T. T. Chen, R. K. Chang, B. L. Laube, *Surface Science* **1983**, *131*, 195-220; bM. A. Tadayyoni, S. Farquharson, M. J. Weaver, *The Journal of Chemical Physics* **1984**, *80*, 1363-1365.

[8] aL. A. Dick, A. D. McFarland, C. L. Haynes, R. P. Van Duyne, *The Journal of Physical Chemistry B* **2002**, *106*, 853-860; bM. Fleischmann, P. J. Hendra, A. J. Mcquillan, *Chem. Phys. Lett.* **1974**, *26*, 163-166.

[9] aM. Abdelsalam, P. N. Bartlett, A. E. Russell, J. J. Baumberg, E. J. Calvo, N. G. Tognalli, A. Fainstein, *Langmuir : the ACS journal of surfaces and colloids* **2008**, *24*, 7018-7023; bV. C. Bassetto, A. E. Russell, L. T. Kubota, P. N. Bartlett, *Electrochim. Acta* **2014**, *144*, 400-405; cR. P. Johnson, J. A. Richardson, T. Brown, P. N. Bartlett, *J. Am. Chem. Soc.* **2012**, *134*, 14099-14107.

[10] L. J. Sherry, S.-H. Chang, G. C. Schatz, R. P. Van Duyne, B. J. Wiley, Y. Xia, *Nano Lett.* **2005**, *5*, 2034-2038.

[11] P. Walstra, *Chem. Eng. Sci.* **1993**, *48*, 333-349.

[12] aG. Zhang, A. S. Cuharuc, A. G. Guell, P. R. Unwin, *Physical chemistry chemical physics : PCCP* **2015**, *17*, 11827-11838; bW. T. E. van den Beld, M. Odijk, R. H. J. Vervuurt, J.-W. Weber, A. A. Bol, A. van den Berg, J. C. T. Eijkel, *Scientific reports* **2017**, *7*, 45080.

[13] K. H. Schmidt, A. Müller, *Coord. Chem. Rev.* **1976**, *19*, 41-97.

[14] R. Zhan, S. Song, Y. Liu, S. Dong, *J Chem Soc Faraday T* **1990**, *86*, 3125-3127.

[15] Y.-E. Miao, H. K. Lee, W. S. Chew, I. Y. Phang, T. Liu, X. Y. Ling, *Chem. Commun.* **2014**, *50*, 5923-5926.

[16] R. P. Johnson, J. A. Richardson, T. Brown, P. N. Bartlett, *J. Am. Chem. Soc.* **2012**, *134*, 14099-14107.

[17] N. G. Tognalli, A. Fainstein, C. Vericat, M. E. Vela, R. C. Salvarezza, *J Phys Chem C* **2008**, *112*, 3741-3746.

[18] H. K. Lee, Y. H. Lee, I. Y. Phang, J. Q. Wei, Y. E. Miao, T. X. Liu, X. Y. Ling, *Angew Chem Int Edit* **2014**, *53*, 5054-5058.

[19] A. J. Bard, L. R. Faulkner, *Electrochemical Methods: Fundamentals and Applications*, Wiley, **2000**.

[20] Z.-Q. Tian, X.-M. Zhang, in *Developments in Electrochemistry*, John Wiley & Sons, Ltd, **2014**, pp. 113-135.

Entry for the Table of Contents (Please choose one layout)

Layout 1:

COMMUNICATION

Plasmonic liquid marble are fabricated from Ag nanocubes to perform as the smallest three dimensional (3D) bifunctional electrochemical (EC) and surface-enhanced Raman scattering platform. Structural changes complement EC data to provide comprehensive mechanism and kinetics elucidation at the microliter scale.

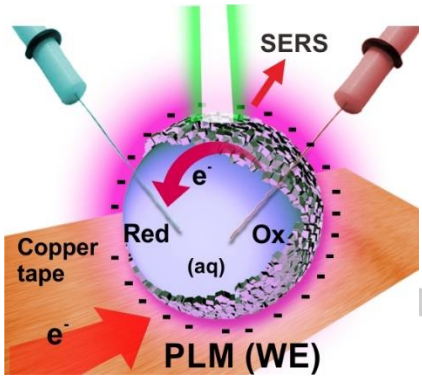

Charlynn Sher Lin Koh, Hiang Kwee Lee, Gia Chuong Phan-Quang, Xuemei Han, Mian Rong Lee, Zhe Yang, Xing Yi Ling

Page No. – Page No.

Electro-activation of microliter-scale reaction within a SERS- and electrically-active three-dimensional Ag shell for molecular-level spectroelectrochemical investigation